

RESEARCH ARTICLE

Dynein-mediated microtubule translocation powering neurite outgrowth in chick and *Aplysia* neurons requires microtubule assembly

Kristi McElmurry¹, Jessica E. Stone¹, Donghan Ma², Phillip Lamoureux³, Yueyun Zhang⁴, Michelle Steidemann⁵, Lucas Fix³, Fang Huang^{2,6,7}, Kyle E. Miller^{3,*} and Daniel M. Suter^{1,7,8,9,*}

ABSTRACT

Previously, we have shown that bulk microtubule (MT) movement correlates with neurite elongation, and blocking either dynein activity or MT assembly inhibits both processes. However, whether the contributions of MT dynamics and dynein activity to neurite elongation are separate or interdependent is unclear. Here, we investigated the underlying mechanism by testing the roles of dynein and MT assembly in neurite elongation of *Aplysia* and chick neurites using time-lapse imaging, fluorescent speckle microscopy, super-resolution imaging and biophysical analysis. Pharmacologically inhibiting either dynein activity or MT assembly reduced neurite elongation rates as well as bulk and individual MT anterograde translocation. Simultaneously suppressing both processes did not have additive effects, suggesting a shared mechanism of action. Single-molecule switching nanoscopy revealed that inhibition of MT assembly decreased the association of dynein with MTs. Finally, inhibiting MT assembly prevented the rise in tension induced by dynein inhibition. Taken together, our results suggest that MT assembly is required for dynein-driven MT translocation and neurite outgrowth.

KEY WORDS: Microtubule, Dynein, Axon, Neurite, Growth cone, Biophysics

INTRODUCTION

Neuronal growth cones are highly motile structures at the distal tips of elongating axons that migrate over distances of microns to meters to connect with precise targets (Lowery and Van Vactor, 2009; Omotade et al., 2017). They steer, advance and retract by detecting a variety of cues, and by continuously reorganizing microtubules (MTs) and filamentous actin (F-actin), cytoskeletal components that are essential for coordinated growth cone motility and guidance (Geraldo and Gordon-Weeks, 2009; Gomez and Letourneau, 2014;


Suter and Forscher, 2000). These polymers drive neurite elongation via specific behaviors that vary across the axon and the three growth cone domains: central (C), transitional (T) and peripheral (P) (Miller and Suter, 2018). Dense MT bundles splay as they extend from the neurite shaft into the growth cone C domain, where they contact F-actin arcs (Dent and Kalil, 2001; Miller and Suter, 2018; Schaefer et al., 2002; Tanaka and Kirschner, 1991). MT looping and catastrophe limit extension beyond this domain, but some pioneer MTs advance into the growth cone P domain, where they encounter F-actin networks (Biswas and Kalil, 2018; Geraldo et al., 2008; Marx et al., 2013; Sanchez-Soriano et al., 2009; Schaefer et al., 2002). F-actin bundles and networks in filopodia and lamellipodia, respectively, push the cell edge forward while generating actomyosin-based tension (Korobova and Svitkina, 2008; Mallavarapu and Mitchison, 1999; Medeiros et al., 2006). F-actin also sweeps MTs backwards during retrograde flow, which mediates the recycling of materials (Lee and Suter, 2008; Schaefer et al., 2002, 2008). The complex interplay of actin dynamics, MT dynamics, MT translocation and related forces is required for neurite outgrowth, but is poorly understood (Miller and Suter, 2018).

MTs have diverse lengths and stability as well as specific orientations within neuronal processes and growth cones (Baas et al., 2016; Kapitein and Hoogenraad, 2015; Miller and Suter, 2018). They polymerize by the addition of tubulin dimers via the energy released through GTP hydrolysis at the plus end, where dynamic catastrophe and rescue behaviors occur (Baas and Black, 1990; Bamberg et al., 1986; Kalil and Dent, 2014; Mitchison and Kirschner, 1984). MT assembly dynamics, along with MT translocation, enable MTs to reorganize and explore the growth cone periphery (Kalil and Dent, 2014; Lee and Suter, 2008; Tanaka et al., 1995; Tanaka and Kirschner, 1991). MT-associated proteins (MAPs) regulate dynamics and translocation to mediate distinct cellular functions, including growth cone steering and advance; they include stabilizing, severing, destabilizing, and plus-end tracking proteins (+TIPs) (Kapitein and Hoogenraad, 2015). Dynein is an important MAP and minus-end oriented organelle motor (Reck-Peterson et al., 2018). *In vitro* reconstitution experiments have shown that dynactin subunit 1 (also known as p150^{Glued}) recruits dynein to MT plus ends, where it tethers MTs to actin, other MTs, and the cellular membrane (Duellberg et al., 2013, 2014; Hendricks et al., 2012; Perlson et al., 2013; Yogev et al., 2017). Other studies have shown that dynein moves MTs anterogradely against actomyosin-generated retrograde forces in the growth cone (Grabham et al., 2007; Myers et al., 2006) and drives bulk MT movement that contributes to neurite elongation (Roossien et al., 2014). Whether this occurs as the result of dynein interacting with dynamic MTs has not been established.

Early studies employing MT assembly inhibitors and MT stabilizing agents suggest that MT assembly at the distal end of

¹Department of Biological Sciences, Purdue University, West Lafayette, IN 47907, USA. ²Weldon School of Biomedical Engineering, Purdue University, West Lafayette, IN 47907, USA. ³Department of Integrative Biology, Michigan State University, East Lansing, MI 48824, USA. ⁴Department of Statistics, Purdue University, West Lafayette, IN 47904, USA. ⁵Department of Pharmacology & Toxicology, Michigan State University, East Lansing, MI 48824, USA. ⁶Purdue Institute of Inflammation, Immunology and Infectious Disease, Purdue University, West Lafayette, IN 47907, USA. ⁷Purdue Institute for Integrative Neuroscience, Purdue University, West Lafayette, IN 47907, USA. ⁸Bindley Bioscience Center, Purdue University, West Lafayette, IN 47907, USA. ⁹Birck Nanotechnology Center, Purdue University, West Lafayette, IN 47907, USA.

*Authors for correspondence (dsuter@purdue.edu; kmiller@msu.edu)

 L.F., 0000-0002-1790-4669; K.E.M., 0000-0003-0401-4736; D.M.S., 0000-0002-5230-7229

the axon is the driving force for axonal elongation (Bamburg et al., 1986; Letourneau and Ressler, 1984). More recently, individual MT translocation and bulk MT movement have been detected in advancing growth cones and elongating neurites (Athamneh et al., 2017; Lee and Suter, 2008; Schaefer et al., 2002). Bulk MT movements occur at slower speeds than individual MT sliding, and correlate with neurite elongation (Athamneh et al., 2017). Therefore, bulk MT movement differs from the individual MT sliding that initiates new neurites (Baas and Yu, 1996; Chang et al., 1998; Lu et al., 2013; Lu and Gelfand, 2017). We recently observed reductions in both docked mitochondrial movement, an indicator of bulk MT advance, and neurite elongation when MT assembly is blocked with nocodazole (Noc) (Athamneh et al., 2017). Similar effects occur when dynein is disrupted (Roossien et al., 2014), which raises questions about how MT assembly, dynein activity and MT translocation are related, and how they contribute to neurite elongation. In this study, we investigated the contributions of these processes to neurite elongation by inhibiting MT assembly with Noc, dynein with ciliobrevin D (CiID), or both in combination, before analyzing neurite growth, dynein–MT localization, MT translocation, MT assembly dynamics and axonal tension. We discovered that inhibiting MT assembly and dynein activity did not have additive effects on neurite growth, suggesting that MT dynamics and translocation are interdependent processes. Specifically, this study indicates that MT assembly is required for dynein to generate individual and bulk MT movements during neurite elongation.

RESULTS

Inhibition of MT dynamics and dynein activity does not produce an additive inhibitory effect on neurite outgrowth

In the present study, we tested the hypothesis that dynein-driven MT movement and MT assembly are interdependent processes in neurite elongation. Dynein inhibition with CiID has previously been shown to inhibit axonal extension of embryonic chick sensory neurons (Roossien et al., 2014; Sainath and Gallo, 2015). To confirm that CiID inhibits dynein in neurons from the sea slug *Aplysia californica*, we assessed its effect on fast mitochondrial transport (Fig. S1). Treatment with 10 μM CiID selectively reduced dynein-mediated retrograde mitochondrial flux by 39% but did not affect anterograde flux. By contrast, 30 μM CiID significantly decreased retrograde mitochondrial flux by 80% and anterograde flux by 77% (Fig. S1), which is consistent with findings in chick neurons (Roossien et al., 2014; Sainath and Gallo, 2015). These results indicate that CiID inhibits dynein in cultured *Aplysia* neurons.

To determine whether MT assembly and dynein-mediated MT translocation are independent or interdependent processes, we chronically inhibited dynein with CiID, blocked MT assembly dynamics with Noc, or simultaneously inhibited both dynein and MT assembly with mixed CiID and Noc treatment. To test for conservation between species, we examined this in both cultured *Aplysia californica* bag cell neurons (Fig. 1A–E) and in chick sensory neurons (Fig. 1F–J). Measurement of *Aplysia* neurite elongation rates by phase contrast microscopy 24 h after plating revealed that Noc alone decreased neurite velocity from $4.4 \pm 0.5 \mu\text{m/h}$ to $-2.9 \pm 0.3 \mu\text{m/h}$, whereas CiID and combined CiID and Noc treatments reduced velocity to $0.0 \pm 0.3 \mu\text{m/h}$ and $-1.1 \pm 0.1 \mu\text{m/h}$, respectively (mean \pm s.e.m.; Fig. 1E). Thus, the neurite retraction caused by Noc treatment was decreased in the presence of CiID. We also quantified the number of primary, secondary and tertiary neurites, and observed a modest reduction in the number of primary and secondary neurites in Noc-containing conditions when

compared to the number observed in the control condition (Ctl; Fig. S2). In chick neurons, drugs were added 4 h after plating, and axonal length was measured 24 h later. The average length of the longest neurite was $98 \pm 5 \mu\text{m}$ in control neurons (Ctl), $54 \pm 4 \mu\text{m}$ in CiID treated neurons, $62 \pm 4 \mu\text{m}$ in Noc treated neurons, and $54 \pm 4 \mu\text{m}$ in CiID+Noc treated neurons (mean \pm s.e.m.; Fig. 1J). The lack of an additive effect of the two drugs in both *Aplysia* and chick neurons suggests that dynein activity and MT assembly are interdependent. This result raised the question of whether inhibition of MT dynamics slows elongation in part by inhibiting the ability of dynein to cause translocation of MTs.

Inhibiting MT assembly dynamics disrupts dynein–MT interactions

Cytoplasmic dynein is a +TIP protein that preferentially binds to growing MT ends (Duellberg et al., 2014). To test whether MT assembly is required for dynein–MT interactions, we immunolabeled cytoplasmic dynein 1 heavy chain 1 and α -tubulin following 5 min applications of 10 μM CiID, 1 μM Noc, or both inhibitors in combination (Fig. 2A–D). Although fewer MTs extended beyond the C domain in Noc-treated growth cones than in controls, MTs in growth cones treated with CiID, either alone or in combination with Noc, extended farther than MTs in growth cones treated with Noc only (Fig. 2A–D). Dynein was detected along MTs in control and CiID-treated growth cones, whereas a significant fraction of the dynein signals were not associated with MTs when MT assembly was inhibited with Noc, either alone or in combination with CiID (Fig. 2A–D).

MT extension and dynein–MT colocalization were quantified for each experimental condition (Fig. 2E,F). MT extension into the P domain was significantly different among all groups (Fig. 2E) ($10.1 \pm 0.6 \mu\text{m}$ in control, $8.1 \pm 0.5 \mu\text{m}$ in CiID, $2.4 \pm 0.4 \mu\text{m}$ in Noc, and $5.1 \pm 0.4 \mu\text{m}$ in CiID+Noc growth cones; mean \pm s.e.m.). Control and CiID growth cones displayed similar numbers of dynein signals per micron of MT ends (Fig. 2F) (0.58 ± 0.03 for controls and 0.50 ± 0.03 for CiID; mean \pm s.e.m.). Noc and combined treatment groups had 0.22 ± 0.02 and 0.28 ± 0.02 dynein signals per micron of MT ends, respectively, which was significantly lower than that observed for control or CiID groups (Fig. 2F). The similar colocalization values for control and CiID groups, along with the twofold decrease in colocalization for Noc- and CiID plus Noc-treated neurons compared to controls, suggest that MT assembly is required for proper dynein–MT interactions. Furthermore, the non-additive negative effects of inhibiting both MT assembly and dynein (Fig. 2E) indicate that MT assembly is required for dynein-mediated MT translocation, and that these processes are interdependent.

Single-molecule switching nanoscopy (SMSN) was performed to confirm the presence of, and gain additional insights into, dynein–MT associations (Fig. 3; Fig. S3). To assess dynein association with MTs, regions of interest containing MTs (300 nm wide and 6 μm long) were extracted from the raw super-resolution images (Fig. 3E). Consistent with epifluorescence analysis, dynein association with MTs was reduced in Noc and CiID plus Noc conditions by 45% and 64% compared to that observed in the control condition ($P=0.01$ and $P<0.001$, respectively; Fig. 3G). Significant differences between the control and CiID conditions were not observed. To analyze dynein distribution as a function of distance from the plus end, the intensity profile of dynein was analyzed for each condition and no significant trends were discovered (Fig. 3F). In conclusion, both conventional and SMSN imaging revealed that inhibiting MT assembly disrupts dynein–MT interactions.

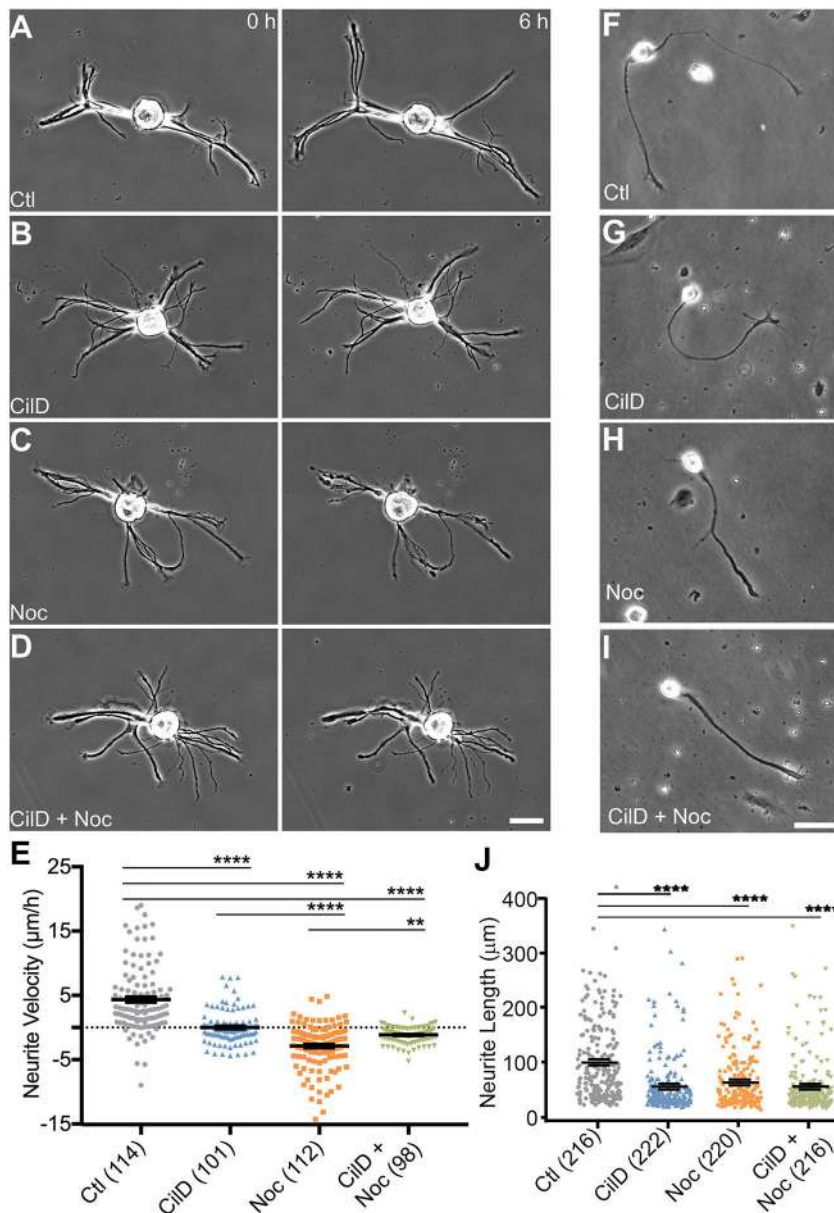


Fig. 1. Inhibition of dynein does not enhance the disruption of neurite outgrowth induced by inhibition of MT assembly. (A–D) Phase contrast images of *Aplysia* bag cell neurons before (0 h) and after 6 h chronic treatments where MT assembly was inhibited by Noc, or dynein was inhibited by CilD, or where both Noc and CilD were used in combination. Scale bar: 50 µm. (E) Although inhibition of either MT assembly or dynein significantly reduces elongation, the effects are not additive. Number of neurites analyzed is shown in parentheses. Plots show mean±s.e.m. for three independent experiments. ** $P<0.01$, **** $P<0.0001$ (one-way ANOVA with Tukey's post hoc test). (F–I) Images of chick sensory neurons 24 h after drug treatment. Scale bar: 50 µm. (J) Although neurite length was significantly shorter in the three drug-treated conditions compared to controls no significant differences were observed between them. Number of neurites analyzed is shown in parentheses. Plots show mean±s.e.m. for three independent experiments. **** $P<0.0001$ (one-way ANOVA with a non-parametric post-hoc Games–Howell test).

MT assembly and dynein activity cooperate during bulk and individual MT translocation

We recently found a strong correlation between bulk MT velocity and neurite growth rates in both *Aplysia* bag cell and chick sensory neurons (Athamneh et al., 2017). Here, we tested the hypothesis that both dynein activity and MT assembly are required for bulk and individual MT translocation and that these processes are interdependent. We injected X-rhodamine-labeled tubulin into bag cell neurons and monitored bulk MT motion for 15 min by fluorescent speckle microscopy (FSM) while tracking the corresponding neurite velocity for 1.5 h by phase contrast microscopy (Fig. 4). MT bulk translocation velocities were measured on kymographs spanning from the growth cone leading edge to 50 µm from the T zone (Fig. 4A–C). The average bulk MT anterograde velocity was 7.3 ± 1.4 µm/h in controls, but velocities were significantly lower in all three drug conditions (CilD, 0.0 ± 0.7 µm/h; Noc, -2.1 ± 0.7 µm/h; combined CilD and Noc, 1.8 ± 0.5 µm/h; mean±s.e.m.) (Fig. 4D). Combinatorial inhibition of MT assembly and dynein did not have an additive effect on bulk MT velocity and was less inhibitory when compared

to the effect of Noc treatment alone (Fig. 4D), which suggests that complex interactions between MT assembly and dynein activity occur. Regression analysis revealed a strong correlation between neurite and bulk MT velocity ($R^2=0.79$; Fig. 5L), which is consistent with our previous study (Athamneh et al., 2017). In conclusion, our results suggest that both MT assembly dynamics and dynein activity are required for anterograde bulk MT translocation and that these processes are interdependent.

Bulk MT movements represent the coordinated motion of MTs cross-linked with MAPs and molecular motors. We hypothesized that MT assembly and dynein activity affect translocation of individual MTs in a similar manner (Fig. 5). To test this hypothesis, we performed individual MT FSM analysis. FSM has previously revealed a significant increase in individual MT anterograde translocation in *Aplysia* growth cones responding to the *Aplysia* cell adhesion molecule apCAM (Lee and Suter, 2008; Schaefer et al., 2008). However, these investigations did not fully define the extent to which individual MT movements contribute to growth cone and neurite advance. In the present study, individual MT

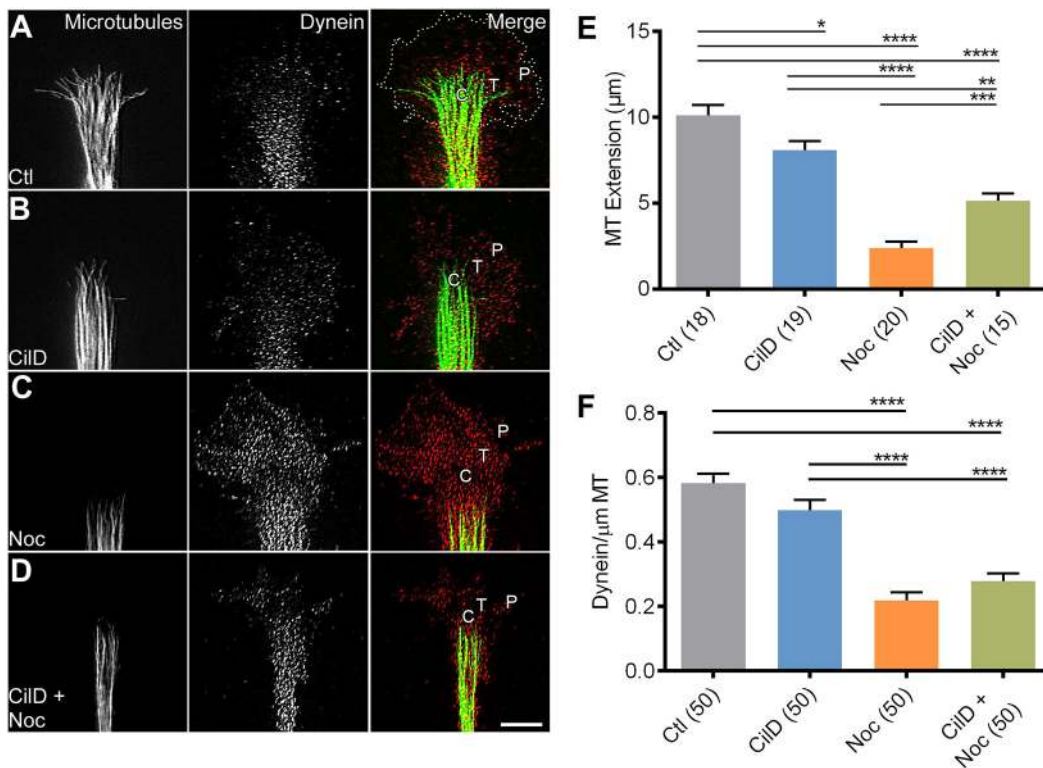


Fig. 2. Inhibiting MT dynamics decreases dynein–MT colocalization. Cultured *Aplysia* neurons were treated with 10 μM CiLD and 1 μM Noc for 5 min before formaldehyde fixation and immunolabeling with antibodies against α -tubulin and dynein heavy chain-1. (A–D) Representative images of growth cones from (A) Control (Ctl), (B) CiLD, (C) Noc and (D) CiLD and Noc conditions. White dashed line in A indicates the leading edge of the growth cone. P, T and C domains are indicated. Scale bar: 10 μm. (E) Quantification of MT extension beyond the C domain boundary. (F) Quantification of dynein signals associated with MT ends. In E and F, the number of growth cones analyzed is shown in parentheses. Quantifications show mean \pm s.e.m. for two independent experiments. * P <0.05, ** P <0.01, *** P <0.001, **** P <0.0001 (one-way ANOVA with Tukey's post hoc test).

analysis revealed that acute Noc and CiLD treatments reduced anterograde MT velocities in the T zone and P domain more than combined CiLD plus Noc treatment (Fig. 5A–G; Fig. S4), which was consistent with chronic treatments (Fig. 1) and bulk MT analysis (Fig. 4). These results indicate that Noc and CiLD do not have additive effects, and MT assembly and dynein-mediated MT translocation are interdependent.

To further analyze individual MT behavior, we calculated the percentage of forward, backward and pause events for individual MTs, and found reduced forward and increased backward events for all drug treatments (Fig. 5H–J). Again, the effects of combinatorial drug treatments on individual MT translocation were compensatory rather than additive, suggesting a complex interaction between MT assembly and dynein-mediated MT translocation. Regression analysis revealed that individual MT velocity correlates less with neurite velocity than with bulk MT velocity (Fig. 5K,L). Taken together, these results indicate MT assembly and dynein-mediated anterograde translocation contribute to MT translocation in an interdependent fashion.

Inhibition of MT assembly disrupts the association of the +TIP protein MACF43

Next, we explored whether dynein inhibition affects MT assembly rates and whether MT assembly modulates associations between +TIPs and MTs. Bag cell neurons were microinjected with mRNA encoding GFP-MACF43, a 43-amino acid fragment of the C-terminal portion of the MT-actin crosslinking factor MACF, that binds to the plus end of MTs (Leung et al., 1999; Sun et al., 2001).

Dynein inhibition with CiLD did not significantly impact MACF comet dynamics (Fig. 6; Movie 1). MT growth velocity was $7.5 \pm 0.3 \mu\text{m}/\text{min}$ in controls and $7.1 \pm 0.3 \mu\text{m}/\text{min}$ in CiLD-treated growth cones, MT growth lengths were nearly the same (control, $2.5 \pm 0.1 \mu\text{m}$; CiLD, $2.4 \pm 0.1 \mu\text{m}$) and there was no significant difference in MT lifetimes (control, $20.2 \pm 0.5 \text{ s}$; CiLD, $20.4 \pm 0.5 \text{ s}$; all values mean \pm s.e.m.) (Fig. 6G–I). Although the percentage of comets that moved in the retrograde direction rose from 13% in controls to 19% in CiLD treated samples, it did not reach statistical significance (Mann–Whitney test; Fig. 6J). In part, the lack of significance occurred due to a single control neuron that had 37% of its comets moving in the retrograde direction, the highest level of retrograde comets in the 34 neurons analyzed. We obtained a P -value of 0.02, when we excluded this neuron from statistical tests. As expected, Noc abolished the GFP–MACF43 signal in less than 5 min, consistent with MACF43 association with growing MTs (Fig. 6E,F). These findings suggest that dynein inhibition does not significantly affect MT growth rates and may modestly increase the percentage of MTs that polymerize retrogradely toward the cell body, whereas disruption of MT assembly inhibits associations between +TIPs and MTs.

Increased axonal tension due to dynein inhibition depends on MT dynamics

We previously demonstrated that inhibiting dynein with CiLD (Roossien et al., 2014) or blocking MT assembly with Noc (Athamneh et al., 2017) increases tension in chick dorsal root ganglion (DRG) axons by similar amounts. If separate mechanisms

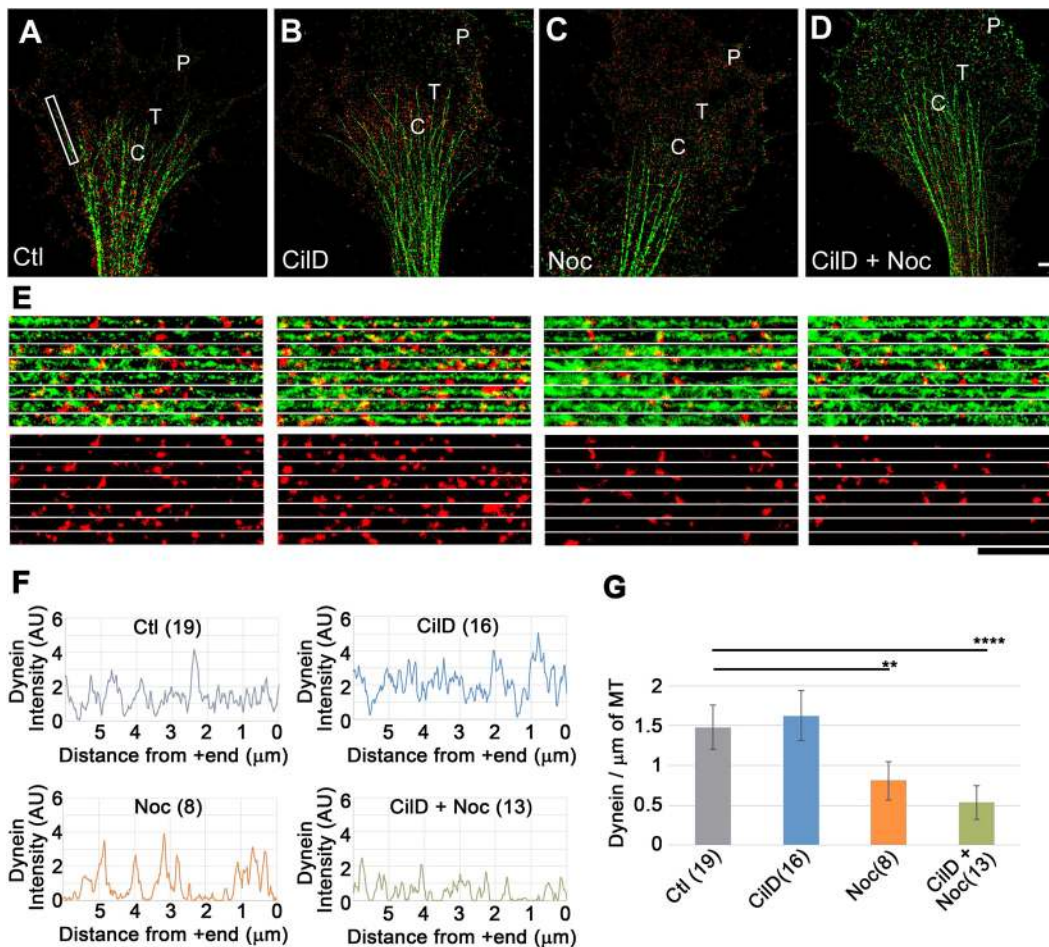


Fig. 3. SMSN confirms that inhibiting MT dynamics decreases dynein–MT colocalization. *Aplysia* neurons were fixed with formaldehyde and immunolabeled with antibodies against α -tubulin and dynein heavy chain-1 following 5 min 10 μ M CiLD and 1 μ M Noc treatments. (A–D) Representative images of MTs (green) and dynein (red) in (A) control (Ctl), (B) CiLD, (C) Noc, (D) CiLD and Noc treated growth cones. The white box shows an example of the cropped regions displayed in E. (E) Enlarged cropped regions of individual MTs and dynein from A–D, with plus ends of MTs aligned to the right. Microtubule and dynein labeling are shown in the top panels while dynein labeling alone is shown in the bottom panels. Scale bars: 2 μ m. (F) Mean dynein distribution as a function of distance from the MT plus end from one experiment. Number of MTs analyzed is shown in parentheses. (G) Dynein association with MTs as a function of drug treatment condition. Number of MTs analyzed is shown in parentheses. Quantification shows mean \pm s.e.m. for one experiment. ** P <0.01, **** P <0.0001 (one-way ANOVA with Tukey's post hoc test).

cause a rise in tension during individual treatments, simultaneous inhibition of dynein activity and MT assembly would be expected to cause a twofold increase in tension compared to individual treatments. Conversely, if MT assembly and dynein activity depend on each other, dynein inhibition would be expected to compensate for a tension rise caused by MT assembly inhibition. To test these hypotheses, embryonic chick DRG growth cones were attached to force-calibrated needles, and forces were allowed to stabilize before CiLD and Noc were added sequentially to the culture medium (Fig. 7A). Tension levels increased twofold upon CiLD treatment (Fig. 7B,C). Rather than rising more, tension decreased significantly following subsequent Noc treatment (Fig. 7B,C). These biophysical results further support the conclusion that MT assembly and dynein-mediated MT movement are interdependent processes.

Several of the previous observations caused by single and combinatorial drug treatments could be in part caused by interactions between the MT and F-actin cytoskeleton. To indirectly assess whether disruption of MTs with nocodazole induces growth cone retraction by altering actomyosin dynamics,

we analyzed the velocity of retrograde actin flow in growth cones of both *Aplysia* bag cell and chick sensory neurons (Fig. S5). As shown in Fig. S5A,B, all three drug conditions significantly reduced retrograde flow in the P domain of *Aplysia* growth cones (control, 5.2 ± 0.7 μ m/min; Noc, 3.2 ± 0.3 μ m/min; CiLD, 3.2 ± 0.3 μ m/min; CiLD+Noc, 2.4 ± 0.3 μ m/min). Furthermore, Noc treatment perturbed the regular shape and organization of filopodia and lamellipodia in the P domain, as revealed by F-actin staining (Fig. S5C). In chick sensory neurons (Fig. S5D,E), the addition of 1.6 μ M nocodazole switched axonal elongation, which occurred at a rate of 29 ± 12 μ m/h, to retraction (-61 ± 43 μ m/h). The velocity of retrograde flow also decreased from 7.5 ± 1.8 μ m/min to 5.8 ± 1.6 μ m/min. More significantly, there was a large decrease in the number of filopodia moving retrogradely. On average, the number of retrograde flow events dropped from 39 ± 6 per hour to 7 ± 5 per hour. Strikingly, in four out of the ten movies, there were no retrograde filopodial movements. These results suggest that nocodazole contributed to the effects on MT translocation and axonal elongation by influencing not only MTs and dynein but also actin organization and dynamics, possibly via actomyosin-driven flow.

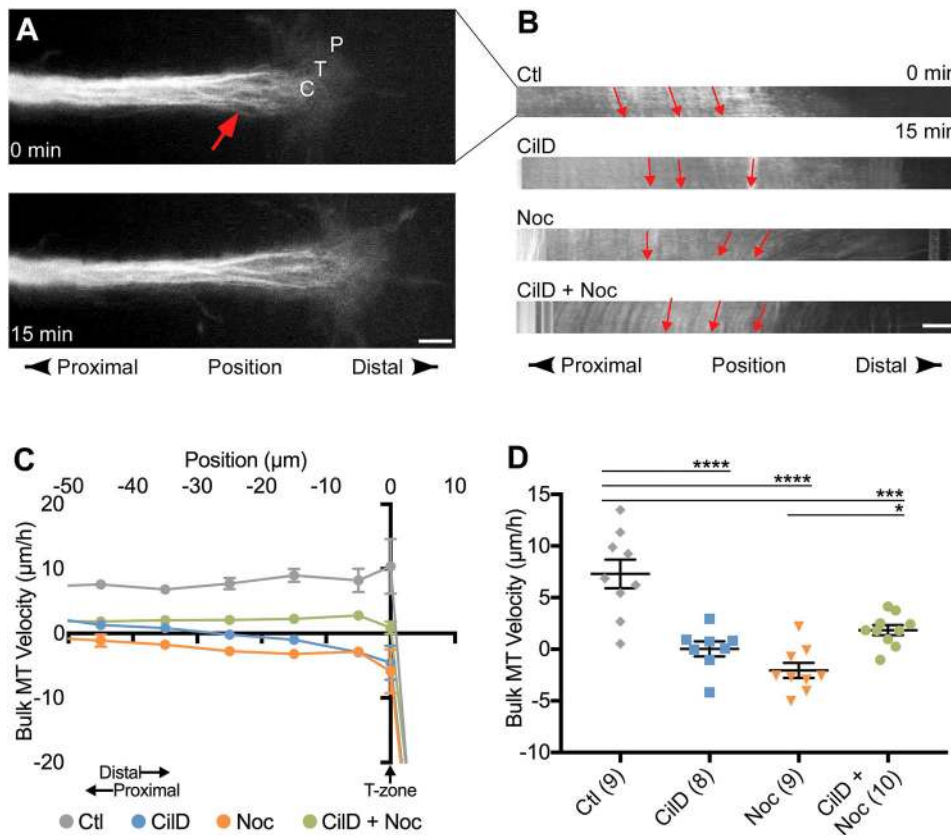


Fig. 4. Bulk MT velocity depends on both MT assembly and dynein activity.

(A) Fluorescence images show MT distribution in an example control neurite at time 0 and 15 min later. The red arrow indicates the region where MTs translocate anterogradely in the control condition. Scale bar: 10 µm. (B) Kymographs of the whole region shown in A, over the 15 min period (vertical axis), show characteristic anterograde velocity in the C domain in the control sample (Ctl) and retrograde velocity in the drug-treated samples (red arrows). Scale bar: 10 µm. (C) Bulk MT velocity as a function of distance from the T zone (set at the origin). Velocities are mean ± s.e.m. for 10 µm regions along the neurite. (D) Bulk MT velocity in the region from 10 to 50 µm proximal of the T zone, shown as mean ± s.e.m. Number of neurons analyzed is shown in parentheses. * $P < 0.05$, *** $P < 0.001$, **** $P < 0.0001$ (one-way ANOVA with Tukey's post hoc test). Data shown in C and D are from eight independent experiments.

DISCUSSION

The necessity of MT assembly for axonal elongation is well established (Coles and Bradke, 2015; Kapitein and Hoogenraad, 2015; Letourneau and Ressler, 1984; Voelzmann et al., 2016). While assembly alone was once considered crucial for outgrowth (Bamburg et al., 1986), recent studies highlight the importance of individual MT sliding during neurite initiation (del Castillo et al., 2015; Lu et al., 2013), rapid MT sliding along growing axons (Baas and Black, 1990; Baas et al., 1991), MT translocation in advancing growth cones responding to adhesion substrates and traction forces (Lee and Suter, 2008; Schaefer et al., 2008), and bulk MT motion during neurite elongation (Athamneh et al., 2017). While MT assembly and translocation have generally been viewed as independent processes, our recent observation that disruption of MT assembly blocks bulk translocation of docked mitochondria in a manner similar to the disruption of dynein (Athamneh et al., 2017; Roossien et al., 2014) raised questions about whether and how MT assembly, dynein activity and MT translocation are interlinked.

Here, we show that attenuating MT assembly and dynein activity concurrently does not have an additive effect on neurite elongation in either *Aplysia* or chick neurons (Fig. 1). This interaction suggested that one of the two processes depends on the other. Because +TIPs recruit dynein to MT plus ends (Coles and Bradke, 2015; Duellberg et al., 2014; Kapitein and Hoogenraad, 2015) and the presence of tyrosinated α -tubulin at the tip of growing microtubules promotes the initiation of dynein–dynactin processive movements (McKenney et al., 2016), it is plausible that dynamic MTs recruit dynein. To test this hypothesis, we performed both conventional and super-resolution imaging of growth cones after inhibiting MT assembly and dynein activity (Figs 2 and 3). Our studies demonstrated that blocking MT assembly reduced both dynein–MT colocalization and MT extension beyond

the C domain. They also showed that dynein inhibition disturbed MT extension less than blocking MT assembly and did not significantly impact dynein–MT colocalization (Figs 2E,F and 3G). Collectively these results suggest that disruption of MT dynamics inhibits neurite elongation in part because it interferes with dynein function. In terms of whether dynein activity affects MT assembly, we observed a strong trend towards the disruption of MT organization following dynein inhibition (Fig. 6). A simple way to interpret this is to consider that the number of MT plus ends that point towards the growth cone decreases upon dynein inhibition. Because MT minus ends are less dynamic than plus ends, CilD treatment could, in part, result in an effect that closely resembles the effect of direct inhibition of MT dynamics. Thus, although we did not observe a direct effect of dynein inhibition on MT dynamics (Fig. 6G–I), indirect effects could underlie the interdependence between MT dynamics and dynein. In light of the finding that in *C. elegans* dynein stabilizes MTs (Yogev et al., 2017), a more systematic analysis of this question is warranted.

Consistent with the results of our previous study, we found a strong correlation between MT translocation and neurite elongation rates (Fig. 5K,L; Athamneh et al., 2017). As with outgrowth, inhibiting either MT assembly or dynein activity alone reduced MT translocation (Figs 4 and 5). Inhibiting both processes at the same time reduced individual MT translocation less than inhibiting MT assembly alone (Fig. 5). The reason dual inhibition with CilD and Noc had a smaller effect than the disruption of dynein or MT assembly alone is unclear. However, this observation raises the possibility that multiple molecular mechanisms couple MTs to retrograde actin flow. Indeed, there is a growing list of proteins that link MTs to F-actin, including the +TIPs (Marx et al., 2013; Neukirchen and Bradke, 2011; Slater et al., 2019). Perturbation of these molecules does not only affect positioning and orientation of

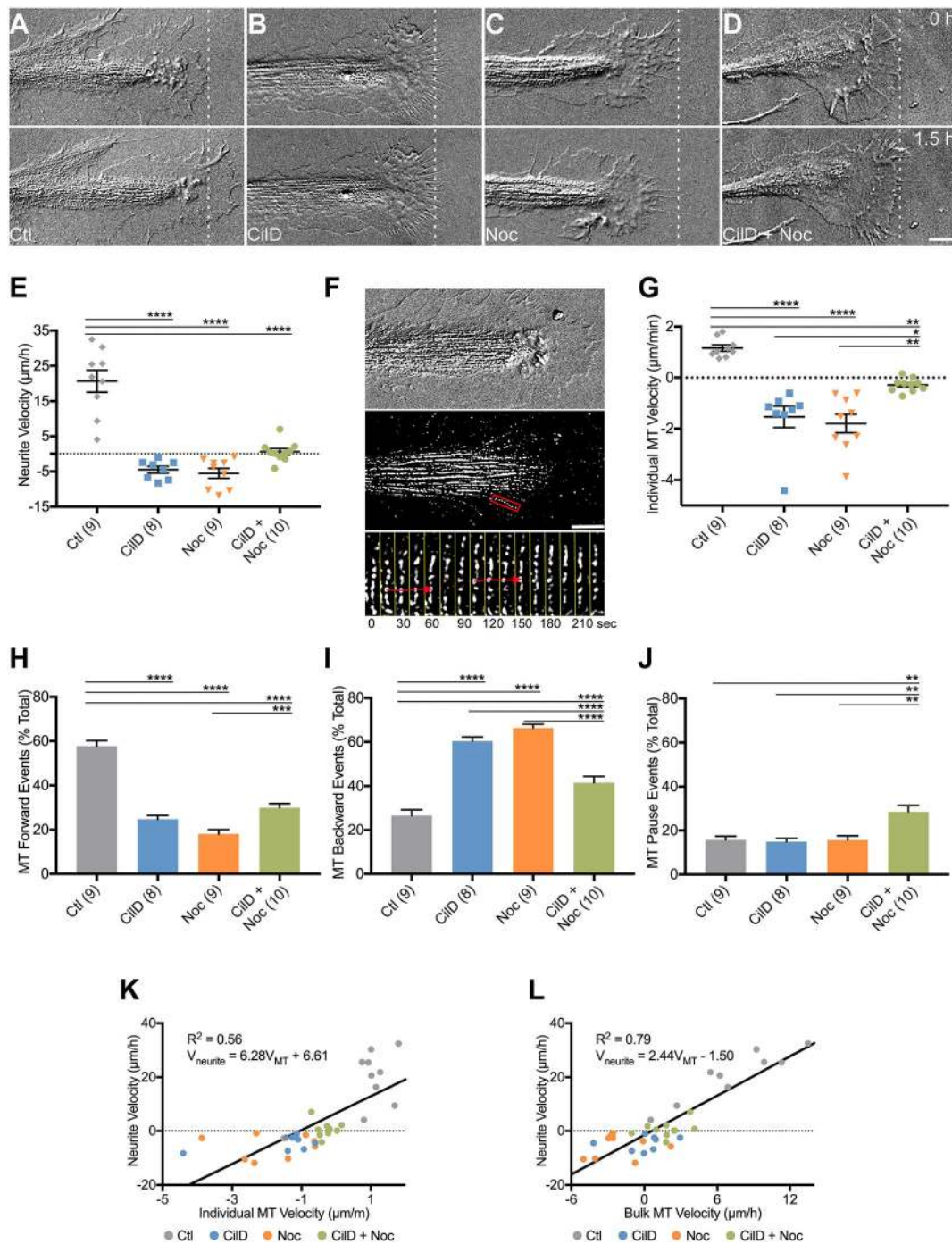


Fig. 5. MT dynamics and dynein activity are interdependent processes in individual MT translocation. (A–D) DIC images portray growth cone morphology and extension before and after 1.5 h treatments with (A) DMSO (control, Ctl), (B) CilD, (C) Noc, (D) CilD and Noc. Dashed white lines show the position of the leading edge at time 0 h. Scale bar: 10 µm. (E) CilD and Noc treatments significantly reduce neurite growth, but the combined treatment has less effect. (F) Growth cone (top), MTs (middle; red box indicates MT depicted in bottom panel), and time-lapse montage, with 15 s intervals, of a single MT labeled with rhodamine–tubulin (bottom). Scale bar: 10 µm. (G) Individual MT velocity. (H–J) Forward, backward, and pause events depicted as a percentage of total MT events. (K) Regression analysis of average individual MT velocity versus axon velocity. Each point represents the velocity of one neurite and the average velocity of five individual MTs. (L) Regression analysis of bulk MT velocity versus neurite velocity. Each point represents the axonal velocity of one neurite and the average bulk MT velocity at a distance of 10 to 50 µm from the T zone. (E, G–L) Data from eight independent experiments. (E, G–J) Number of neurons analyzed is shown in parentheses. Quantifications show means ± s.e.m. * $P < 0.05$, ** $P < 0.01$, *** $P < 0.001$, **** $P < 0.0001$ [(E, G–I) one-way ANOVA with Tukey's post hoc test, (J) Mann–Whitney test]. (G–J) Values are the average of five MTs for each neuron.

MTs but also influences the organization of the F-actin cytoskeleton and ultimately neurite growth and guidance.

We built upon our previous biophysical experiments to further investigate relationships between MT dynamics and dynein-driven translocation with respect to axonal tension. Classical studies have

demonstrated that MT disruption increases axonal tension (Joshi et al., 1985) and have led to the longstanding idea that MT assembly generates a pushing force that counteracts actomyosin contraction to drive neurite elongation (Buxbaum and Heidemann, 1992). Our recent studies show that inhibition of dynein induces bulk MT

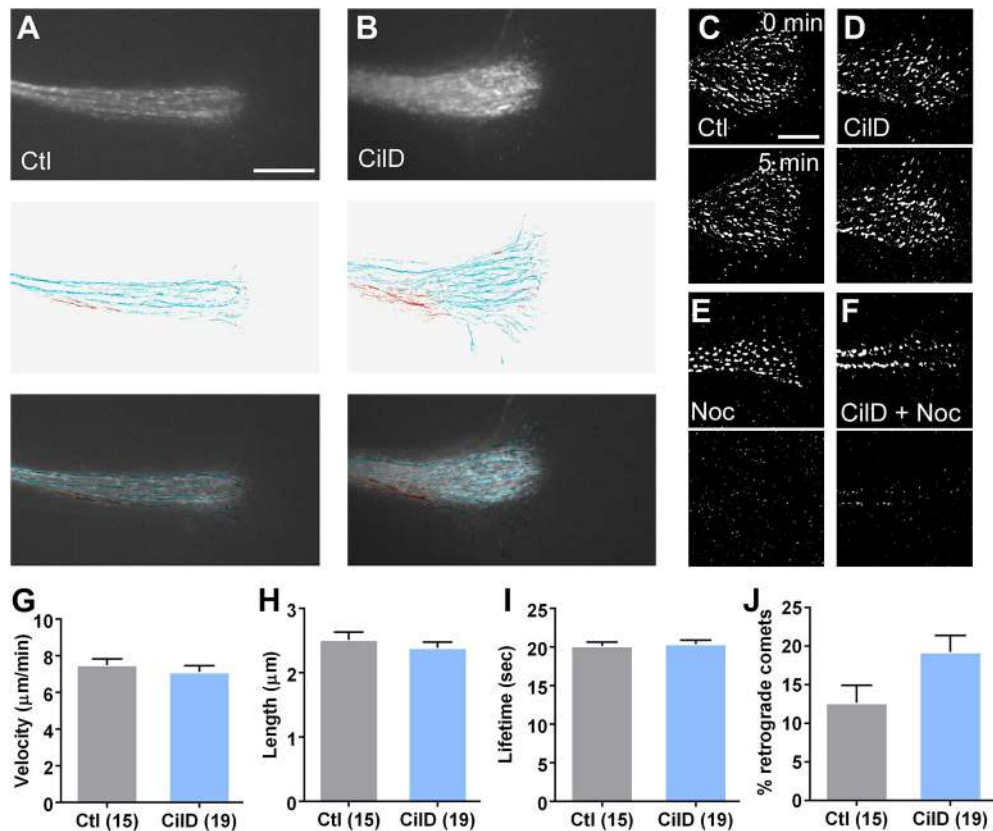


Fig. 6. Inhibition of dynein causes a mild increase in MT polarity reversal but does not affect plus end MT dynamics. (A,B) Top, fluorescence images of the +TIP marker GFP-MACF43 used to track MT assembly. Middle, tracks of comet motion in the anterograde (light blue) and retrograde (red) directions. Bottom, overlay of tracks on the fluorescence image. Scale bar 25 μm . To assess the effects of dynein disruption, CiID was added at a concentration of 10 μM for 5 min. Images from control conditions (Ctl) are shown in A, and images taken following CiID treatment are shown in B. Retrograde comet movements increase, as illustrated by the increase in the number of red tracks. (C–F) GFP-MACF43-positive comets from processed images at 0 min (top) and 5 min (bottom) following treatment with DMSO control (C), 10 μM CiID (D), 1 μM Noc (E), or a combination of 10 μM CiID and 1 μM Noc (F). Noc treatment alone, or in combination with CiID treatment, leads to a rapid loss in MACF association with MTs. Scale bar 10 μm . (G–J) CiID has no significant effect on comet velocity, run length or comet lifetime, but increases the percentage of retrograde comets ($P=0.06$, Mann–Whitney test). Data shown are mean \pm s.e.m. from ten independent experiments. Numbers in parentheses represent the number of neurons analyzed for each condition.

retraction and increases axonal tension (Athamneh et al., 2017; Roossien et al., 2014). These observations have led to a working model where dynein inhibition increases tension because dynein extensile force generation does not counteract actomyosin contractile forces (Ahmad et al., 2000; Myers et al., 2006; Roossien et al., 2014). In the present study, axonal tension increased with CiID treatment; however, tension dramatically decreased upon subsequent Noc application (Fig. 7). To better understand this response, we examined the effect of Noc on growth cone dynamics and actin organization. Noc treatment induced a significant drop in retrograde actin flow in both model systems and a reduction in the frequency of filopodial retraction events in chick neurons (Fig. S5). Although additional studies are required to explain this response, one possibility is that, in addition to disrupting dynein, inhibition of MT assembly alters actin dynamics and the generation of actin-based traction forces. Taken together these results raise the possibility that tension increases when MT assembly is disrupted, in part because dynein-mediated force generation decreases, while traction forces generated at the growth cone simultaneously decrease. Collectively, this helps explain the exquisite sensitivity of growth cones to drugs that alter MT dynamics (Bamburg et al., 1986). Finally, some of the Noc-mediated effects on actin organization and dynamics could also be in part due to effects on MTs regulating substrate-cytoskeletal coupling, as shown by Suter et al. (2004).

We propose a model that consists of three force-generating mechanisms to explain our results (Fig. 8; Movies 2–4). Along the axon, actomyosin generates a contractile force that pulls the growth cone rearwards. Dynein generates an opposing, extensile force that pushes MTs forward. Non-muscle myosin II pulls the P-domain rearward and the C-domain forward across the T zone. Rapid elongation occurs under control conditions when the forward push of dynein combined with the forward pull of the growth cone exceeds the rearward pull of actomyosin in the axon (Fig. 8A). Dynein disruption leads to retraction and a rise in tension because it prevents counteraction of axonal contractile force generation (Fig. 8B; Movie 2). Disruption of MT assembly with Noc has a similar effect because it causes dynein to disassociate from MTs (Fig. 8C; Movie 3). It follows that simultaneous inhibition of dynein activity and MT assembly do not have an additive inhibitory effect on elongation (Fig. 8D; Movie 4). Additionally, reduced retrograde actin flow, induced by both CiID and nocodazole (Fig. S5), may increase retraction by decreasing traction force generation.

MATERIALS AND METHODS

Aplysia neuronal cell culture

Aplysia californica bag cell neurons were cultured in L-15 medium (41300-039, Invitrogen) supplemented with artificial sea water (ASW) (400 mM NaCl, 9 mM CaCl_2 , 27 mM MgSO_4 , 28 mM MgCl_2 , 4 mM L-glutamine,

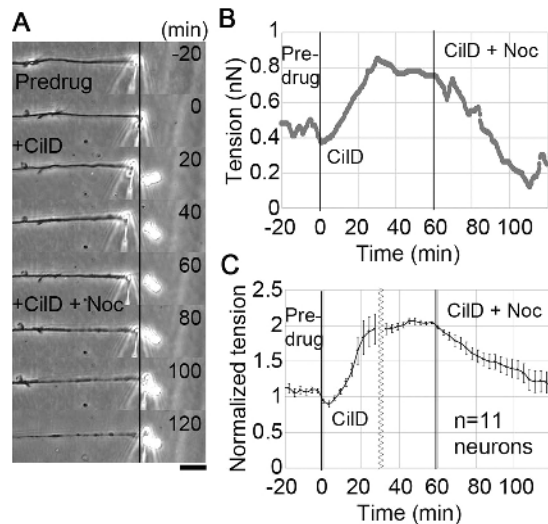


Fig. 7. Inhibition of MT assembly abolishes the rise in axonal tension induced by dynein inhibition. (A) Representative phase contrast images of the tension assay. Chick DRG axons were attached to force-calibrated towing needles, and tension was allowed to stabilize for at least 20 min. Dynein was then inhibited with 100 μ M CiID for at least 1 h, before MT assembly was disrupted with 1.6 μ M Noc. Scale bar: 10 μ m. (B) Tension levels for the neuron shown in panel A over 2 h. (C) Mean \pm 95% c.i. of normalized tension from 11 independent experiments. Because duration of CiID treatment before addition of Noc varied from 1 to 2 h, data were aligned separately based on the times of CiID and combined CiID and Noc application. The wavy line denotes the discontinuity between the two alignments.

50 μ g/ml gentamicin and 5 mM HEPES, pH 7.9) on coverslips or glass dishes coated with 20 μ g/ml poly-L-lysine (P6282, Sigma-Aldrich, St Louis, MO) in hemolymph after overnight digestion in dispase (D4693, Sigma-Aldrich), as reported previously (He et al., 2015). Neurons were incubated overnight at 14°C before experimentation.

Chick DRG neuronal cell culture

Chick DRG neurons dissected from 11-day-old embryos were plated on poly-ornithine-coated tissue culture dishes as previously described (Lamoureux et al., 2010). All animal experiments were performed according to approved guidelines. The dishes were prepared by covering with 0.01% poly-L-ornithine solution (A-004-M, Sigma-Aldrich) for 30 min then rinsing with sterile ultrapure water. Dissociated ganglion cells were added to the dishes and grown overnight at 37°C in L-15 medium supplemented with 0.6% glucose, 200 mM glutamine, 10% fetal bovine serum, 100 U/ml penicillin, 136 μ g/ml streptomycin sulfate, N9 growth supplement, and 25 ng/ml nerve growth factor, pH 7.1.

Pharmacological treatments of *Aplysia* neurons

Cells were treated with 0.1% DMSO for controls, 1 μ M nocodazole (Noc; M1404, Sigma-Aldrich), 10 μ M ciliobrevinD (CiID; 250401, Sigma-Aldrich), or a combination of 10 μ M CiID and 1 μ M Noc in the cell culture medium. CiID or Noc treatments were applied for 6 h at 23°C for chronic studies and for 5 min at 23°C for acute studies. Combined treatments were performed similarly, but CiID was applied for 5 min before Noc to ensure dynein inhibition before MT assembly inhibition for both chronic and acute treatments. *Aplysia* neuronal cultures were maintained at 14°C for 6 h before imaging at 23°C during chronic treatments. For acute treatments, cells were maintained at 23°C for the 1.5 h duration of the experiment. Immunostaining studies followed the acute treatment scheme before fixation.

Aplysia neurite outgrowth analysis

A Nikon TE2000 E2 Eclipse inverted microscope with an iXon Ultra 888 EMCCD camera (Oxford Instruments) was used to image *Aplysia* neurons in L-15-ASW at room temperature. For chronic treatment studies, neurons

were imaged using a 10 \times phase objective with an additional 1.5 \times magnification lens before drug applications and \sim 6 h afterward to obtain neurite growth data. MetaMorph 7.8 (Molecular Devices) and ImageJ (NIH) were used to measure neurite lengths and numbers. Neurite velocity was determined for each individual neurite by dividing the length difference achieved over 6 h by the corresponding time. Three independent experiments were performed. SAS (SAS 9.4, SAS Institute, Inc.) was used for statistical testing (one-way ANOVA with Tukey's post hoc test).

Chick DRG outgrowth analysis

At 4 h after plating, Noc and/or CiID were added to chick sensory neurons. After 24 h, images were acquired using a 20 \times phase objective on a Leica DM IRB microscope with an ORCA-ER camera (Hamamatsu) using μ Manager software (Open Imaging). The longest axon for isolated neurons was measured using the freehand line and measure tools in ImageJ. Data were exported to Excel and then Minitab 19 for statistical analysis. Because the length distributions were non-normal, significance was tested using a one-way ANOVA with a non-parametric post-hoc Games-Howell test, which is similar to the Tukey test but does not assume equal variance.

Immunostaining

Aplysia cells were fixed with 3.7% formaldehyde in ASW supplemented with 400 mM sucrose for 15 min. They were permeabilized with 0.05% saponin in fixative for 10 min before washing in 0.005% saponin in phosphate-buffered saline (PBS). Blocking was performed with 10% bovine albumin serum in PBS containing 0.005% saponin for 1 h. Samples were incubated for 3 h with antibodies against the 532 kDa dynein heavy chain-1 (101452, GeneTex) and the 52 kDa α -tubulin subunit (MA1-80189, Thermo Fisher Scientific) in blocking buffer at 1:250 dilution. Preparations were washed prior to incubating with Alexa Fluor 568-conjugated anti-IgG antibodies (A-11077, Invitrogen) to label MTs and Alexa Fluor 647-conjugated anti-IgG antibodies (A-21244, Invitrogen) to label dynein at 1:250 in PBS containing 0.005% saponin for 1 h. Samples were washed, and post-fixation was performed with 3.7% formaldehyde in ASW with 400 mM sucrose for 5 min before a final wash. All immunostaining procedures were conducted at room temperature. Fixed cells were imaged in PBS containing 0.005% saponin.

Dynein-MT colocalization and MT extension analysis

MetaMorph 7.8 was used for image processing and MT extension analysis (Fig. 2E). MT extension was determined as the MT lengths between the C domain boundary and the MT ends in the P domain, and then averaged to calculate an extension value for each growth cone. For dynein-MT colocalization analysis of conventional fluorescence images, the two channels were overlaid in ImageJ, and the number of dynein signals overlapping with the MT ends (5–10 μ m) were determined by manual counting (Fig. 2F).

Single-molecule switching nanoscopy

Super-resolution imaging was performed using a custom-built apparatus on an Olympus IX-73 microscope stand (IX-73, Olympus America Inc.) with a 100 \times 1.35 NA silicone oil-immersion objective lens (FV-U2B714, Olympus America Inc.) and a PIFOC objective positioner (ND72Z2LAQ, Physik Instrumente). Samples were excited with a 642 nm laser (2RU-VFL-P-2000-642-B1R, MPB Communications Inc.) or a 560 nm laser (2RU-VFL-P-500-560, MPB Communications Inc.). Both lasers were focused on the back aperture of the objective lens and offset from the optical axis to illuminate the sample in highly inclined thin illumination mode (Tokunaga et al., 2008). The filter turret contained a quad-band dichroic mirror (Di03-R405/488/561/635-t1, Semrock Inc.). Relay lenses in 4f alignment produced a final magnification of \sim 54 at a scientific complementary metal-oxide-semiconductor camera (Orca-Flash4.0v3, Hamamatsu) with an effective pixel size of 120 nm. A filter wheel containing two bandpass filters (FF01-731/137-25 and FF01-600/52-25, Semrock Inc.) was placed just before the camera. Single-molecule localization was performed as described previously (Huang et al., 2013). Imaging was conducted for \sim 20 cycles for MTs and 5 cycles for dynein, with 2000 frames per cycle.

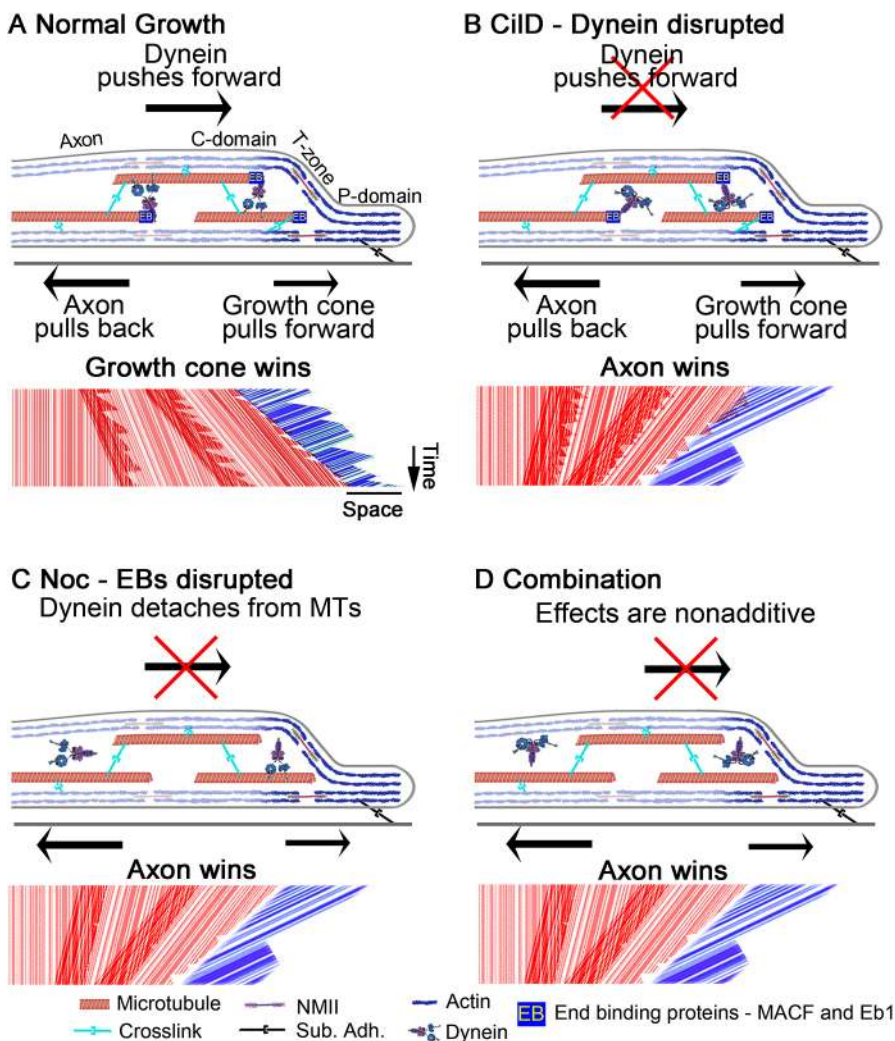


Fig. 8. MT assembly and dynein-mediated MT translocation are interdependent activities required for neurite elongation. (A) Schematic of normal neurite outgrowth showing a side view of the growth cone. In the model, dynein generates an extensile force on the MT array that promotes elongation, the tension generated in the axon pulls the growth cone rearward, and the traction forces produced by retrograde flow pull MTs in the C-domain forward. The kymograph illustrates the forward advance and dynamics of MTs in red, and the rearward flow of actin in blue (Movies 2–4). (B) Disruption of dynein activity alone decreases its forward push on the MT array. Consequently, the tension generated in the axon overcomes the forward pull of the growth cone, and the axon retracts (Movie 2). (C) Disruption of MT assembly causes the loss of end-binding protein (EB) association, which decreases the association of dynein with MTs. Extensile forces decrease, and the axon pulls the growth cone rearwards (Movie 3). (D) Disruption of MT assembly and dynein activity in combination does not have an additive negative effect, because disruption of MTs directly impairs force generation by dynein (Movie 4).

For dual channel alignment, coverslips with immunostained cells were incubated for 20 min with 100 nm red fluorescent beads (F8801, Thermo Fisher Scientific) diluted to 1:100,000. Samples were washed three times with PBS, and then coverslips were placed in a chamber (A7816, Thermo Fisher Scientific) with 600 μ l of imaging buffer [10% (w/v) glucose in 50 mM Tris-HCl (JT4109-02, Avantor), 50 mM NaCl (S271-500, Thermo Fisher Scientific), 10 mM cysteamine hydrochloride (M6500-25G, Sigma-Aldrich), 50 mM thioethylene glycol (M3148-25ML, Sigma-Aldrich), 2 mM cyclooctatetraene (138924-1G, Sigma-Aldrich), 2.5 mM protocatechuic acid (37580-25G-F, Sigma-Aldrich) and 50 nM protocatechuate 3,4-dioxygenase, pH 8.0 (P8279-25UN, Sigma-Aldrich)] topped with a layer of mineral oil (124020010, Acros Organics). Channels were merged, and images were aligned using ImageJ software.

Dynein–MT colocalization analysis based on SMSN images

To determine the distribution of dynein as a function of distance, 20-pixel wide (\sim 300 nm) traces of MTs and dynein were selected from the raw SMSN images in ImageJ using the freehand line tool and straightened using the straighten function. The dynein channel of the individual images was converted into a montage with the plus ends of MTs aligned. The montage was cropped to include the last 6 μ m of the MTs, and the plot profile function of ImageJ was used to measure average pixel intensity as a function of distance. To measure the average density of dynein per micrometer of MT, the spots in the dynein channel of the montages were counted and divided by MT length. The raw data are shown in Fig. S3.

MT fluorescent speckle microscopy

Aplysia neurons were injected with 1 mg/ml X-rhodamine-labeled tubulin in buffer (TL620M-A, BST01-001; Cytoskeleton Inc.) 1 day after plating as

previously described (Lee and Suter, 2008). Tubulin was centrifuged at 13,000 *g* for 30 min and stored on ice before injections. Microinjection pipettes (1B100F-4, World Precision Instruments) were prepared using a Narishige PP830 vertical system and chilled to 4°C before use. Cells recovered for a minimum of 1 h at 14°C before drug treatments. Cells were imaged immediately following MT time-lapse recordings and \sim 1.5 h later, using similar imaging conditions, to obtain neurite growth data for acute treatment investigations. Time-lapse recordings were obtained on a Nikon TE2000 E2 Eclipse inverted microscope equipped with an iXon Ultra 888 EMCCD camera using a 60 \times 1.4 numerical aperture (NA) oil immersion DIC objective with 1.5 \times additional magnification for 15 min at 15 or 20 s intervals.

Speckle processing and individual MT analysis

Images were processed using MetaMorph 7.8 low-pass and Laplace filters as described previously (Lee and Suter, 2008). Individual MT translocation events and rates were measured by producing montages from processed images and tracing internal fluorescent speckles over time. Velocities of five MTs extending from the growth cone T zone into the P domain were averaged to report individual MT velocities for each cell.

MT bulk velocity analysis

The line tool in ImageJ was used to trace a centerline from the distal tip of an axon to the leading edge of the growth cone on fluorescent image stacks. The width of the region incorporated the whole growth cone and axon. The region was then cropped and straightened before applying Gaussian blur and Mexican hat filters for image processing. Kymographs were produced, and velocities were traced in ImageJ. Velocities were then divided into 10 μ m sections along the axon to calculate regional averages.

MACF43 mRNA injections and +TIP analysis

The mMESSAGE mMACHINE SP6 Transcription kit (AM1340, Thermo Fisher Scientific) was used to obtain mRNA from GFP-MACF43 constructs in the pCS2+ vector (construct kindly provided by Dr Laura Anne Lowery, Boston College, Chestnut Hill, MA). This construct includes 43 residues at the C-terminus of MACF2, which binds to EB1 (Honnappa et al., 2009). RNA was mixed with TE buffer (AM9860, Ambion) to 0.8–1 mg/ml GFP-MACF43 mRNA concentration, spun at 13,000 *g* for 30 min, and stored on ice before injection into *Aplysia* neurons. Microinjection pipettes (1B100F-4, World Precision Instruments) were prepared using a Narishige PP830 vertical system and chilled to 4°C before use. Cells recovered for 5 h at 14°C before acute treatments, as described in pharmacological methods. MACF recordings were conducted in accordance with the time-lapse protocol described for MT fluorescent speckle microscopy, except images were acquired for 5 min at 3 s intervals. U-track MATLAB software was used to analyze MACF43 comet dynamics (R2018b, The MathWorks, Inc.) (Applegate et al., 2011; Jaqaman et al., 2008).

Analysis of fast axonal transport of mitochondria in *Aplysia* neurons

To label mitochondria, *Aplysia* bag cell neurons were treated for 15 min with 100 nM MitoTracker Red CM-HSXRos (M7512, Molecular Probes) in L-15-ASW medium, which was then replaced with fresh medium. 1 h after labeling, neurons were treated with DMSO control, 10 μ M CiD, or 30 μ M CiD for 10 min. Following the drug treatment, neurons were imaged using a 60 \times 1.4 NA objective every 3 s. Because the thickness of *Aplysia* neurons generates kymographs that are difficult to image, multi-kymographs were generated with 0.7 μ m thick regions (5 pixels thick) that were z-projected using the maximum projection function in ImageJ. This generated 5–15 kymographs per axon. A line was drawn down the center of the kymographs and flux was calculated by counting the number of mitochondria that passed the line in each direction. The raw flux was then divided by the observation time and the width of the axon to yield flux in units of mitochondria/ μ m min. Velocity was calculated based on the slope of the trace as a mitochondrion passed the center line. Flux and velocity were imported into Minitab and analyzed by one-way ANOVA using Games–Howell Pairwise comparison.

Retrograde flow analysis

Aplysia neurons underwent acute 5 min pharmacological treatments as explained above, and time-lapse recordings were obtained for 10 min at 3 s intervals using a 60 \times 1.4 numerical aperture oil immersion DIC objective on a Nikon TE2000 E2 Eclipse inverted microscope equipped with an iXon Ultra 888 EMCCD camera. Following time lapse recordings, MetaMorph 7.8 was used to process the image sequences using low-pass and Laplace filters. Kymographs were made using the processed image sequences, and the line tool in MetaMorph was used to trace retrograde flow over time on the kymograph to obtain the average retrograde velocity of actin. Chick sensory neurons were cultured on glass coverslips coated with 0.01% poly-ornithine solution for 1 h at room temperature, rinsed 3 \times with sterile H₂O, and then coated with 20 μ g/ml laminin for 20 min. Images were acquired at 10 s intervals for 20 min, 1.6 μ M nocodazole added, and imaging continued for at least 25 min. Kymographs were constructed by using a minimum intensity z-projection in ImageJ. Retrograde flow was measured by tracking the motion of filopodia and lamellipodia in kymographs. Velocity was determined from the slope of traces and the retrograde flow events per hour were calculated by dividing the number of traces by the duration of observation. Growth rate was calculated based on the change in position of the phase-dense region of the growth cone over the pre-drug and post-drug acquisition periods. Significance was calculated in Excel using a two-tailed paired Student's *t*-test.

Chick DRG neuronal tension assay

Experiments were performed on a Leica DM IRB inverted microscope on a Vibraplane (Kinetics Systems) vibration isolation table. Chick neuronal cultures were maintained at 37°C with an air-curtain stage heater. Images (taken using a 40 \times magnification objective) were captured at 20 s intervals with a Hamamatsu Orca-ER digital camera controlled by ImageJ Micromanager. A force-calibrated needle was attached to an advancing

growth cone. Preparation and force calibration of towing needles has been previously described (Lamoureux et al., 2011). Micropipettes were coated with 0.01% poly-ornithine (Sigma-Aldrich) for 30 min, followed by a 1 mg/ml concanavalin A solution for 30 min. The growth cone was attached to the coated needle and lifted off the substrate to allow firm attachment to the needle. After attachment, the growth cone was brought down near the dish to achieve a better focus plane, and time-lapse imaging was initiated. Once tension equilibrium was established for a minimum of 10 min, CiD in 0.5 ml of L-15 medium was added to the dish to a final concentration of 100 μ M. An average of 1 h was allowed to pass to establish a new tension equilibrium before adding Noc in 0.5 ml medium for a final concentration of 1.6 μ M. The tension response was observed for 40 min to 1 h thereafter.

Data analysis and display

Data were gathered and analyzed as described for specific experiments throughout. SAS (SAS 9.4, SAS Institute, Inc.), SPSS (IBM SPSS Statistics 25.0, IBM), and Excel (02981-002-423991, Microsoft) software were used for statistical analysis. GraphPad Prism (GraphPad 7.0d, GraphPad Software, Inc.) was used for data displays.

Acknowledgements

We are grateful to Dr Laura Anne Lowery and her laboratory (Boston College, Chestnut Hill, MA) for providing the GFP-MACF43 construct for MT +TIP labeling and for their advice on GFP-MACF43 imaging and analysis. We are also thankful to the Suter laboratory members who provided insights and expertise, especially Yuan Ren, Aslihan Terzi, and Ahmad Athamneh.

Competing interests

The authors declare no competing or financial interests.

Author contributions

Conceptualization: K.M., Y.Z., F.H., K.E.M., D.M.S.; Methodology: K.M., D.M., P.L., Y.Z., M.S., L.F., F.H., K.E.M., D.M.S.; Software: K.E.M.; Validation: K.M., J.E.S., D.M., F.H., K.E.M., D.M.S.; Formal analysis: K.M., J.E.S., D.M., P.L., Y.Z., M.S., L.F., F.H., K.E.M., D.M.S.; Investigation: K.M., J.E.S., D.M., P.L., M.S., L.F., K.E.M.; Resources: K.M., F.H., K.E.M., D.M.S.; Data curation: K.M., D.M.S.; Writing - original draft: K.M.; Writing - review & editing: K.M., J.E.S., D.M., F.H., K.E.M., D.M.S.; Visualization: K.M., D.M., F.H., K.E.M., D.M.S.; Supervision: F.H., K.E.M., D.M.S.; Project administration: F.H., K.E.M., D.M.S.; Funding acquisition: F.H., K.E.M., D.M.S.

Funding

This work was enabled by funding from National Science Foundation 1146944-IOS (to D.M.S.), National Science Foundation 0951019-IOS and National Institutes of Health 1R01MH094607-01A1 (to K.M.), National Institutes of Health R35 GM119785 and Defense Advanced Research Projects Agency D16AP00093 (to F.H.). Deposited in PMC for release after 12 months.

Supplementary information

Supplementary information available online at <http://jcs.biologists.org/lookup/doi/10.1242/jcs.232983.supplemental>

References

- Ahmad, F. J., Hughey, J., Wittmann, T., Hyman, A., Greaser, M. and Baas, P. W. (2000). Motor proteins regulate force interactions between microtubules and microfilaments in the axon. *Nat. Cell Biol.* **2**, 276–280. doi:10.1038/35010544
- Applegate, K. T., Besson, S., Matov, A., Bagonis, M. H., Jaqaman, K. and Danuser, G. (2011). plusTipTracker: quantitative image analysis software for the measurement of microtubule dynamics. *J. Struct. Biol.* **176**, 168–184. doi:10.1016/j.jsb.2011.07.009
- Athamneh, A. I. M., He, Y., Lamoureux, P., Fix, L., Suter, D. M. and Miller, K. E. (2017). Neurite elongation is highly correlated with bulk forward translocation of microtubules. *Sci. Rep.* **7**, 7292. doi:10.1038/s41598-017-07402-6
- Baas, P. W. and Black, M. M. (1990). Individual microtubules in the axon consist of domains that differ in both composition and stability. *J. Cell Biol.* **111**, 495–509. doi:10.1083/jcb.111.2.495
- Baas, P. W. and Yu, W. Q. (1996). A composite model for establishing the microtubule arrays of the neuron. *Mol. Neurobiol.* **12**, 145–161. doi:10.1007/BF02740651
- Baas, P. W., Slaughter, T., Brown, A. and Black, M. M. (1991). Microtubule dynamics in axons and dendrites. *J. Neurosci. Res.* **30**, 134–153. doi:10.1002/jnr.490300115

- Baas, P. W., Rao, A. N., Matamoros, A. J. and Leo, L.** (2016). Stability properties of neuronal microtubules. *Cytoskeleton* **73**, 442-460. doi:10.1002/cm.21286
- Bamburg, J. R., Bray, D. and Chapman, K.** (1986). Assembly of microtubules at the tip of growing axons. *Nature* **321**, 788-790. doi:10.1038/321788a0
- Biswas, S. and Kalil, K.** (2018). The microtubule-associated protein tau mediates the organization of microtubules and their dynamic exploration of actin-rich Lamellipodia and Filopodia of cortical growth cones. *J. Neurosci.* **38**, 291-307. doi:10.1523/JNEUROSCI.2281-17.2017
- Buxbaum, R. E. and Heidemann, S. R.** (1992). An absolute rate theory model for tension control of axonal elongation. *J. Theor. Biol.* **155**, 409-426. doi:10.1016/S0022-5193(05)80626-5
- Chang, S. H., Rodionov, V. I., Borisov, G. G. and Popov, S. V.** (1998). Transport and turnover of microtubules in frog neurons depend on the pattern of axonal growth. *J. Neurosci.* **18**, 821-829. doi:10.1523/JNEUROSCI.18-03-00821.1998
- Coles, C. H. and Bradke, F.** (2015). Coordinating neuronal actin-microtubule dynamics. *Curr. Biol.* **25**, R677-R691. doi:10.1016/j.cub.2015.06.020
- del Castillo, U., Winding, M., Lu, W. and Gelfand, V. I.** (2015). Interplay between kinesin-1 and cortical dynein during axonal outgrowth and microtubule organization in *Drosophila* neurons. *eLife* **4**, e10140. doi:10.7554/eLife.10140
- Dent, E. W. and Kalil, K.** (2001). Axon branching requires interactions between dynamic microtubules and actin filaments. *J. Neurosci.* **21**, 9757-9769. doi:10.1523/JNEUROSCI.21-24-09757.2001
- Duellberg, C., Fourniol, F. J., Maurer, S. P., Roostalu, J. and Surrey, T.** (2013). End-binding proteins and Ase1/PRC1 define local functionality of structurally distinct parts of the microtubule cytoskeleton. *Trends Cell Biol.* **23**, 54-63. doi:10.1016/j.tcb.2012.10.003
- Duellberg, C., Trokter, M., Jha, R., Sen, I., Steinmetz, M. O. and Surrey, T.** (2014). Reconstitution of a hierarchical +TIP interaction network controlling microtubule end tracking of dynein. *Nat. Cell Biol.* **16**, 804-811. doi:10.1038/ncb2999
- Geraldo, S. and Gordon-Weeks, P. R.** (2009). Cytoskeletal dynamics in growth-cone steering. *J. Cell Sci.* **122**, 3595-3604. doi:10.1242/jcs.042309
- Geraldo, S., Khanzada, U. K., Parsons, M., Chilton, J. K. and Gordon-Weeks, P. R.** (2008). Targeting of the F-actin-binding protein drebrin by the microtubule plus-tip protein EB3 is required for neuriteogenesis. *Nat. Cell Biol.* **10**, 1181-1189. doi:10.1038/ncb1778
- Gomez, T. M. and Letourneau, P. C.** (2014). Actin dynamics in growth cone motility and navigation. *J. Neurochem.* **129**, 221-234. doi:10.1111/jnc.12506
- Grabham, P. W., Seale, G. E., Bennecib, M., Goldberg, D. J. and Vallee, R. B.** (2007). Cytoplasmic dynein and LIS1 are required for microtubule advance during growth cone remodeling and fast axonal outgrowth. *J. Neurosci.* **27**, 5823-5834. doi:10.1523/JNEUROSCI.1135-07.2007
- He, Y. P., Ren, Y., Wu, B. B., Decourt, B., Lee, A. C., Taylor, A. and Suter, D. M.** (2015). Src and cortactin promote lamellipodia protrusion and filopodia formation and stability in growth cones. *Mol. Biol. Cell* **26**, 3229-3244. doi:10.1091/mbc.e15-03-0142
- Hendricks, A. G., Lazarus, J. E., Perelson, E., Gardner, M. K., Odde, D. J., Goldman, Y. E. and Holzbaur, E. L. F.** (2012). Dynein tethers and stabilizes dynamic microtubule plus ends. *Curr. Biol.* **22**, 632-637. doi:10.1016/j.cub.2012.02.023
- Honnappa, S., Gouveia, S. M., Weisbrich, A., Damberger, F. F., Bhavesh, N. S., Jawhari, H., Grigoriev, I., van Rijssel, F. J., Buey, R. M., Lawera, A., Jelesarov, I., Winkler, F. K., Wüthrich, K., Akhmanova, A., Steinmetz, M. O.** (2009). An EB1-binding motif acts as a microtubule tip localization signal. *Cell* **138**, 366-376. doi:10.1016/j.cell.2009.04.065
- Huang, F., Hartwich, T. M. P., Rivera-Molina, F. E., Lin, Y., Duim, W. C., Long, J. J., Uchil, P. D., Myers, J. R., Baird, M. A., Mothes, W. et al.** (2013). Video-rate nanoscopy using sCMOS camera-specific single-molecule localization algorithms. *Nat. Methods* **10**, 653-658. doi:10.1038/nmeth.2488
- Jaqaman, K., Loerke, D., Mettlen, M., Kuwata, H., Grinstein, S., Schmid, S. L. and Danuser, G.** (2008). Robust single-particle tracking in live-cell time-lapse sequences. *Nat. Methods* **5**, 695-702. doi:10.1038/nmeth.1237
- Joshi, H. C., Chu, D., Buxbaum, R. E. and Heidemann, S. R.** (1985). Tension and compression in the cytoskeleton of PC 12 Neurites. *J. Cell Biol.* **101**, 697-705. doi:10.1083/jcb.101.3.697
- Kalil, K. and Dent, E. W.** (2014). Branch management: mechanisms of axon branching in the developing vertebrate CNS. *Nat. Rev. Neurosci.* **15**, 7-18. doi:10.1038/nrn3650
- Kapitein, L. C. and Hoogenraad, C. C.** (2015). Building the neuronal microtubule cytoskeleton. *Neuron* **87**, 492-506. doi:10.1016/j.neuron.2015.05.046
- Korobova, F. and Svitkina, T.** (2008). Arp2/3 complex is important for filopodia formation, growth cone motility, and neurogenesis in neuronal cells. *Mol. Biol. Cell* **19**, 1561-1574. doi:10.1091/mbc.e07-09-0964
- Lamoureux, P., Heidemann, S. R., Martzke, N. R. and Miller, K. E.** (2010). Growth and elongation within and along the axon. *Dev. Neurobiol.* **70**, 135-149. doi:10.1002/dneu.20764
- Lamoureux, P., Heidemann, S. and Miller, K. E.** (2011). Mechanical manipulation of neurons to control axonal development. *J. Vis. Exp.* **50**, e2509. doi:10.3791/2509
- Lee, A. C. and Suter, D. M.** (2008). Quantitative analysis of microtubule dynamics during adhesion-mediated growth cone guidance. *Dev. Neurobiol.* **68**, 1363-1377. doi:10.1002/dneu.20662
- Letourneau, P. C. and Ressler, A. H.** (1984). Inhibition of neurite initiation and growth by taxol. *J. Cell Biol.* **98**, 1355-1362. doi:10.1083/jcb.98.4.1355
- Leung, C. L., Sun, D., Zheng, M., Knowles, D. R. and Liem, R. K. H.** (1999). Microtubule actin cross-linking factor (MACF): a hybrid of dystonin and dystrophin that can interact with the actin and microtubule cytoskeletons. *J. Cell Biol.* **147**, 1275-1285. doi:10.1083/jcb.147.6.1275
- Lowery, L. A. and Van Vactor, D.** (2009). The trip of the tip: understanding the growth cone machinery. *Nat. Rev. Mol. Cell Biol.* **10**, 332-343. doi:10.1038/nrm2679
- Lu, W. and Gelfand, V. I.** (2017). Moonlighting motors: kinesin, dynein, and cell polarity. *Trends Cell Biol.* **27**, 505-514. doi:10.1016/j.tcb.2017.02.005
- Lu, W., Fox, P., Lakonishok, M., Davidson, M. W. and Gelfand, V. I.** (2013). Initial neurite outgrowth in *Drosophila* neurons is driven by kinesin-powered microtubule sliding. *Curr. Biol.* **23**, 1018-1023. doi:10.1016/j.cub.2013.04.050
- Mallavarapu, A. and Mitchison, T.** (1999). Regulated actin cytoskeleton assembly at filopodium tips controls their extension and retraction. *J. Cell Biol.* **146**, 1097-1106. doi:10.1083/jcb.146.5.1097
- Marx, A., Godinez, W. J., Tsimashchuk, V., Bankhead, P., Rohr, K. and Engel, U.** (2013). *Xenopus* cytoplasmic linker-associated protein 1 (XCLASP1) promotes axon elongation and advance of pioneer microtubules. *Mol. Biol. Cell* **24**, 1544-1558. doi:10.1091/mbc.e12-08-0573
- McKenney, R. J., Huynh, W., Vale, R. D. and Sirajuddin, M.** (2016). Tyrosination of α -tubulin controls the initiation of processive dynein-dynactin motility. *EMBO J.* **35**, 1175-1185. doi:10.15252/embj.201593071
- Medeiros, N. A., Burnette, D. T. and Forscher, P.** (2006). Myosin II functions in actin-bundle turnover in neuronal growth cones. *Nat. Cell Biol.* **8**, 215-226. doi:10.1038/ncb1367
- Miller, K. E. and Suter, D. M.** (2018). An integrated cytoskeletal model of neurite outgrowth. *Front. Cell. Neurosci.* **12**, 19. doi:10.3389/fncel.2018.00447
- Mitchison, T. and Kirschner, M.** (1984). Microtubule assembly nucleated by isolated centrosomes. *Nature* **312**, 232-237. doi:10.1038/312232a0
- Myers, K. A., Tint, I., Nadar, C. V., He, Y., Black, M. M. and Baas, P. W.** (2006). Antagonistic forces generated by cytoplasmic dynein and myosin-II during growth cone turning and axonal retraction. *Traffic* **7**, 1333-1351. doi:10.1111/j.1600-0854.2006.00476.x
- Neukirchen, D. and Bradke, F.** (2011). Cytoplasmic linker proteins regulate neuronal polarization through microtubule and growth cone dynamics. *J. Neurosci.* **31**, 1528-1538. doi:10.1523/JNEUROSCI.3983-10.2011
- Omotade, O. F., Pollitt, S. L. and Zheng, J. Q.** (2017). Actin-based growth cone motility and guidance. *Mol. Cell. Neurosci.* **84**, 4-10. doi:10.1016/j.mcn.2017.03.001
- Perelson, E., Hendricks, A. G., Lazarus, J. E., Ben-Yaakov, K., Gradus, T., Tokito, M. and Holzbaur, E. L. F.** (2013). Dynein interacts with the Neural Cell Adhesion Molecule (NCAM180) to tether dynamic microtubules and maintain synaptic density in cortical neurons. *J. Biol. Chem.* **288**, 27812-27824. doi:10.1074/jbc.M113.465088
- Reck-Peterson, S. L., Redwine, W. B., Vale, R. D. and Carter, A. P.** (2018). The cytoplasmic dynein transport machinery and its many cargoes. *Nat. Rev. Mol. Cell Biol.* **19**, 382-398. doi:10.1038/s41580-018-0004-3
- Roossien, D. H., Lamoureux, P. and Miller, K. E.** (2014). Cytoplasmic dynein pushes the cytoskeletal meshwork forward during axonal elongation. *J. Cell Sci.* **127**, 3593-3602. doi:10.1242/jcs.152611
- Sainath, R. and Gallo, G.** (2015). The dynein inhibitor Ciliobrevin D inhibits the bidirectional transport of organelles along sensory axons and impairs NGF-mediated regulation of growth cones and axon branches. *Dev. Neurobiol.* **75**, 757-777. doi:10.1002/dneu.22246
- Sanchez-Soriano, N., Travis, M., Dajas-Bailador, F., Goncalves-Pimentel, C., Whitmarsh, A. J. and Prokop, A.** (2009). Mouse ACF7 and *Drosophila* short stop modulate filopodia formation and microtubule organization during neuronal growth. *J. Cell Sci.* **122**, 2534-2542. doi:10.1242/jcs.046268
- Schaefer, A. W., Kabir, N. and Forscher, P.** (2002). Filopodia and actin arcs guide the assembly and transport of two populations of microtubules with unique dynamic parameters in neuronal growth cones. *J. Cell Biol.* **158**, 139-152. doi:10.1083/jcb.200203038
- Schaefer, A. W., Schoonderwoert, V. T. G., Ji, L., Medeiros, N., Danuser, G. and Forscher, P.** (2008). Coordination of actin filament and microtubule dynamics during neurite outgrowth. *Dev. Cell* **15**, 146-162. doi:10.1016/j.devcel.2008.05.003
- Slater, P. G., Cammarata, G. M., Samuelson, A. G., Magee, A., Hu, Y. and Lowery, L. A.** (2019). XMAP215 promotes microtubule-F-actin interactions to regulate growth cone microtubules during axon guidance in *Xenopus laevis*. *J. Cell Sci.* **132**, jcs224311. doi:10.1242/jcs.224311
- Sun, D. M., Leung, C. L. and Liem, R. K. H.** (2001). Characterization of the microtubule binding domain of microtubule actin crosslinking factor (MACF): identification of a novel group of microtubule associated proteins. *J. Cell Sci.* **114**, 161-172.
- Suter, D. M. and Forscher, P.** (2000). Substrate-cytoskeletal coupling as a mechanism for the regulation of growth cone motility and guidance. *J. Neurobiol.* **44**, 97-113. doi:10.1002/1097-4695(200008)44:2<97::AID-NEU2>3.0.CO;2-U

- Suter, D. M., Schaefer, A. W. and Forscher, P.** (2004). Microtubule dynamics are necessary for Src family kinase-dependent growth cone steering. *Curr. Biol.* **14**, 1194-1199. doi:10.1016/j.cub.2004.06.049
- Tanaka, E. M. and Kirschner, M. W.** (1991). Microtubule behavior in the growth cones of living neurons during axon elongation. *J. Cell Biol.* **115**, 345-363. doi:10.1083/jcb.115.2.345
- Tanaka, E., Ho, T. and Kirschner, M. W.** (1995). The role of microtubule dynamics in growth cone motility and axonal growth. *J. Cell Biol.* **128**, 139-155. doi:10.1083/jcb.128.1.139
- Tokunaga, M., Imamoto, N. and Sakata-Sogawa, K.** (2008). Highly inclined thin illumination enables clear single-molecule imaging in cells (vol 5, pg 159, 2008). *Nat. Methods* **5**, 455-455. doi:10.1038/nmeth0508-455
- Voelzmann, A., Hahn, I., Pearce, S. P., Sánchez-Soriano, N. and Prokop, A.** (2016). A conceptual view at microtubule plus end dynamics in neuronal axons. *Brain Res. Bull.* **126**, 226-237. doi:10.1016/j.brainresbull.2016.08.006
- Yogev, S., Maeder, C. I., Cooper, R., Horowitz, M., Hendricks, A. G. and Shen, K.** (2017). Local inhibition of microtubule dynamics by dynein is required for neuronal cargo distribution. *Nat. Commun.* **8**, 15063. doi:10.1038/ncomms15063